Fundus Image Transformation Revisited: Towards Determining More Accurate Registrations

Danilo Motta
ICMC
University of São Paulo (USP)
São Carlos, Brazil
daniloam@icmc.usp.br

Wallace Casaca
Energy Engineering Department
São Paulo State University (UNESP)
Rosana, Brazil
wallace.coc@gmail.com

Afonso Paiva
ICMC
University of São Paulo (USP)
São Carlos, Brazil
apeneto@icmc.usp.br

***Abstract*—Image registration is an important pre-processing step in several computer vision applications, being crucial in medical imaging systems where patients are examined and diagnosed almost exclusively by images. For fundus images, in which microscopic differences are significant to better support medical decisions, an accurate registration is imperative. Historically, geometric transformations derived from quadratic models have been widely used as a benchmark to perform registration on fundus images, but in this paper, we demonstrate that quadratic and other high-order mappings are not necessarily the best choices for this purpose, even for well-established state-of-the-art registration methods. From a novel overlapping metric designed to determine the best image transformation that maximizes the registration accuracy, we improve the assertiveness of several methods of the literature while still preserving the same computational burden initially reached by those methods.**

***Keywords*- fundus image; registration; transformation; accuracy**

I. INTRODUCTION

The process of mapping a given image onto another image of the same scene is popularly known as *image registration* [1]. This procedure is commonly applied by many medical imaging systems where images captured at different times, scales and lighting conditions need to be carefully processed and aligned to ensure more consistency in clinical examinations. In fact, the efficacy in preventing eye's diseases as well as to prescribe more comprehensive diagnostics highly depend on the success of those computer applications to perform registration accurately, specially when dealing with fundus images. Moreover, computer-aided medical technologies have become a trend in the planning of optical surgeries as well [2].

Despite the benefits and advances promoted by computer-guided diagnostics, one must observe that the methods used to effectively compute the registration models on fundus images can produce inaccurate outputs in many pragmatic cases, or even totally fail in this task, thus reducing the effective performance of several automatized registration systems, as previously reported by [3], [4], [5]. To properly attempt overcoming this problem, a tremendous number of image registration techniques have been proposed in the last few decades, which vary in terms of many different resources [6], [7], [1], [8], [9], [10], [11], [12], [13]. Metrics for accuracy validation have also been considered in this context [14], [15], [16], in an effort to check the real impact of existing registration tools while still making sure that clinical requirements will be strictly satisfied by those tools.

While the plurality of the image registration methods has strongly contributed to the progress of general computer-aided applications over the years, an important issue not always covered by most existing registration methods is the choice of the best candidate for the geometric alignment function. Indeed, the methods assume as quadratic the transformation used to accomplish the alignment between the retinal images [1], [8]. To better illustrate this process, Figure 1 shows a typical situation where a quadratic mapping is applied on two fundus images, resulting in an inaccurate alignment, as highlighted by the rightmost result. In summary, by taking quadratic/spherical transformations to register fundus images in the majority of cases, one could be discarding potential mapping candidates for which the registration accuracies are higher. Moreover, from a more suitable geometric transformation, one could be able to deal with several cases of unregistered images where classic alignment functions cannot succeed as expected.

In this paper we investigate how to choose optimal transformations through a robust and user-independent decision metric which improves the accuracy performance of several state-of-the-art registration algorithms on eye fundus images. From a novel overlapping metric specifically designed to select the best image transformation, i.e., the one that maximizes the registration accuracy, we improve the performance of well-established registration methods while still maintaining their current computational costs. In more specific terms, the proposed metric consists in checking topological and geometric changes in the eye's blood vessels and it does not require for ground truth in practical usages, being also computed in real-time even for large images commonly found in medical contexts, also serving as a useful index to support registration applications at interactive rates.

In summary, the main contributions of this paper are:

- Our study demonstrates that no transformation is optimal for fundus registration: the ideal mapping varies according to the retinal image pair.
- A new metric that gauges the overlapping between fundus images, called here as *Gain Coefficient*.
- An effective methodology to select the best transformation candidate for the registration task.
- Our approach is simple-to-code and user-independent, has low computational cost and improves the accuracy of several popular image registration methods.

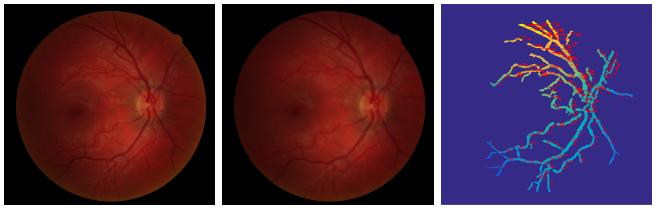

(a) (b) (c)

Figure 1. Setting quadratic transformations to register fundus images: (a) reference image, (b) target image and (c) a representative vessel graph showing the distortion after the geometric mapping between the images. The vector sizes reflect the difference between the corresponding nodes located at both left and middle eye's blood vessels. The redder the graph branches, the more prominent is the alignment distortion.

II. Transformation Models

We consider four well-known transformation models in our analysis: *similarity*, *affine*, *homography* and *quadratic*. Notice that, although we take the above-mentioned geometric models as a baseline, the approach presented here can be applied for other sets of transformations as well. Next, we briefly describe each one of these transformations.

Points in the projective plane. Points in Euclidean plane can be represented in the *projective plane* $\mathbb{P}^2 = \mathbb{R}^3 \setminus (0,0,0)^\top$ using homogeneous coordinates $\tilde{\mathbf{x}} = (\tilde{x}, \tilde{y}, \tilde{w})^\top$. Moreover, a given point $\tilde{\mathbf{x}} \in \mathbb{P}^2$ can be transformed back to Euclidean plane by dividing through by the last entry, i.e.,

$$\tilde{\mathbf{x}} = (\tilde{x}, \tilde{y}, \tilde{w})^\top = \tilde{w}\left(\frac{\tilde{x}}{\tilde{w}}, \frac{\tilde{y}}{\tilde{w}}, 1\right)^\top = \tilde{w}(x, y, 1)^\top = \tilde{w}\overline{\mathbf{x}}\,,$$

where $\overline{\mathbf{x}} = (x, y, 1)^\top$ is the augmented vector of $\mathbf{x} = (x, y)^\top \in \mathbb{R}^2$.

Similarity transformation. This transformation can be written as $\mathbf{x}' = s\,\mathbf{R}_\theta\,\mathbf{x} + \mathbf{t}$, where s is a scale factor, $\mathbf{R}_\theta$ accounts for the rotation matrix by an angle θ, and $\mathbf{t} = (t_x, t_y)^\top$ determines the translation vector. The geometric mapping is properly computed as:

$$\mathbf{x}' = \begin{bmatrix} \cos\theta & -\sin\theta & t_x \\ \sin\theta & \cos\theta & t_y \end{bmatrix} \overline{\mathbf{x}}\,.$$

Affine transformation. In two-dimensional coordinate systems, the affine transformation is determined by $\mathbf{x}' = \mathbf{A}\overline{\mathbf{x}}$, where $\mathbf{A}$ is an arbitrary 2×3 augmented matrix. This matrix is known as *affine transformation matrix*.

Projective transformation. Also called *perspective* or *homography mapping* [17], this transformation is computed through homogeneous coordinates $\tilde{\mathbf{x}}' = \tilde{\mathbf{H}}\tilde{\mathbf{x}}$, where $\tilde{\mathbf{H}}$ is a 3×3 matrix. The resulting vector $\tilde{\mathbf{x}}'$ in homogeneous coordinates can be converted to $\mathbf{x}' = (x', y')^\top \in \mathbb{R}^2$ by:

$$x' = \frac{h_{11}x + h_{12}y + h_{13}}{h_{31}x + h_{32}y + h_{33}} \quad \text{and} \quad y' = \frac{h_{21}x + h_{22}y + h_{23}}{h_{31}x + h_{32}y + h_{33}}\,.$$

Quadratic transformation. The quadratic transformation is a second order polynomial function which is defined as: $\mathbf{x}' = \mathbf{B}\,\mathbf{p}(\mathbf{x}) + \mathbf{A}\overline{\mathbf{x}}$, where $\mathbf{A}$ and $\mathbf{B}$ are 2×3 matrices, and $\mathbf{p}(\mathbf{x}) = (x^2, y^2, xy)^\top$.

Notice that the matrices that appear in the geometric transformations are defined so as to allow the use of a specific registration method. Considering some particular differences between these transformations, similarity-based preserves angles between lines, affine-based ensures that parallel lines will be kept after the geometric alignment, projective-based conserves straight lines and, finally, quadratic-based can embed lines into the curved shape of the retina, but it also introduces non-linear errors, as shown in [18].

The reader can observe that the only non-linear mapping considered in our analysis is the quadratic one. In fact, this is the most common choice when coping with fundus images [1], [8]. Its use is endorsed by the spherical shape of the eye, but one may note that non-linear transformations can also lead to non-linear errors. For instance, the monitoring of some pathologies, including glaucoma, is accomplished from a sequence of eye's exams, so these errors can influence the diagnostic if they were not taken into account.

In the following, we present a simple methodology to determine the best geometric transformation for a given pair of fundus images.

III. Determining Optimal Maps for Registration

In order to carefully choose the best geometric mapping which maximizes the accuracy for a given registration method, we apply the following sequence of steps:

- S.1 Extract the blood vessels from the fundus image pair I_R and I_M, creating two new binary images, B_R and B_M (for more details, see [19]);
- S.2 Compute each transformation i (if possible) to the image to be mapped, B_M, generating a set of transformed images $T_i(B_M)$;
- S.3 For each collection of images $(B_R, B_M, T_i(B_M))$, compute the registration accuracy based on a new overlapping metric, called *Gain Coefficient* (GC);
- S.4 The optimal geometric transformation is the one that maximizes the GC.

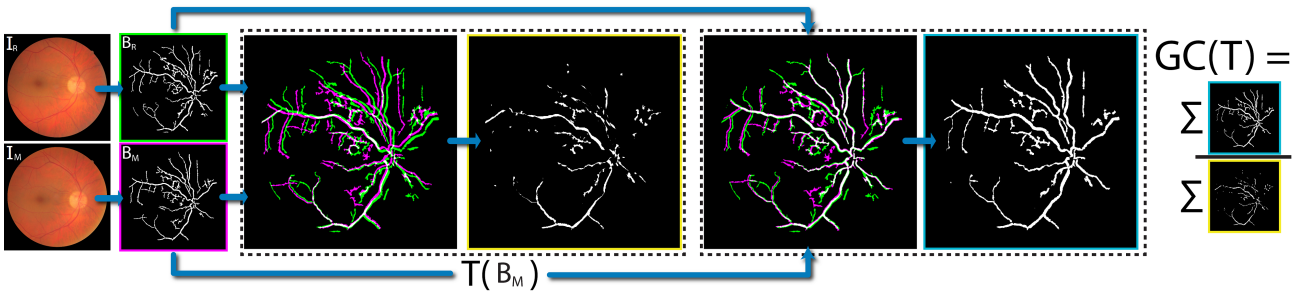

Figure 2. Measuring the registration accuracy from the GC metric. First, blood vessels B_R and B_M are built from the fundus images I_R and I_M. Then, a geometric transformation model T is applied on B_M so as to generate $T(B_M)$. Finally, the Gain Coefficient is computed as in Equation (1).

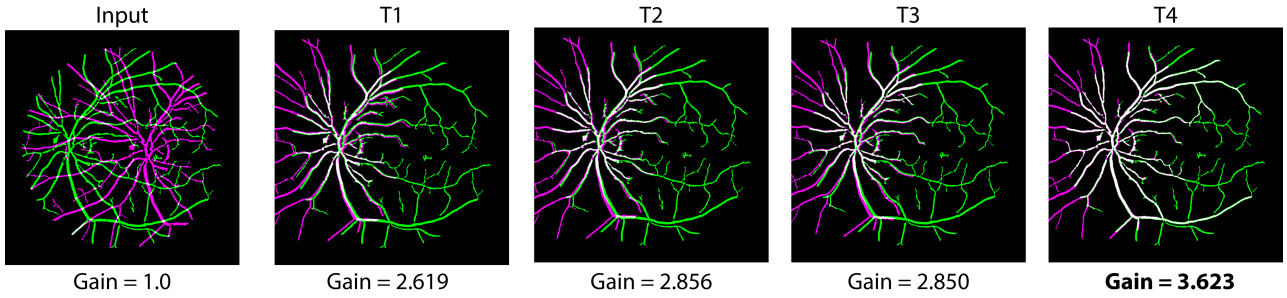

Figure 3. Illustration of our GC-based approach for selecting the optimal transformation. GC is calculated for each collection of binary images $(B_R, B_M, T_i(B_M)), i = 1, 2, 3, 4$, being in this example the mapping function T_4 chosen by our scheme.

The rationale behind our approach is quite simple: no exclusive transformation is optimal, i.e. the mapping depends on the image pair as well as the matching points given by the registration method. For this purpose, we maximize the GC for all the available transformations, which is computationally inexpensive and can be computed "on-the-fly". Finally, the proposed GC metric that quantifies the registration accuracy for a given transformation T is computed as follows:

$$GC(B_R, B_M, T) = \frac{|B_R \cap T(B_M)|}{|B_R \cap B_M|}. \qquad (1)$$

Equation (1) states that if a geometric transformation aligns more pixels after the mapping, GC will be greater than 1, as the numerator indicates the amount of overlapped pixels on B_R and $T(B_M)$, while $B_R \cap B_M$ quantifies the input overlap wherein no transformation is applied. Figure 2 illustrates how the GC properly works while Figure 3 shows an illustrative case covering the steps S.4 and S.5 of our selection criterion. Notice from the graphical sketches that we depict composed images where B_R is set in the green channel, B_M (or $T(B_M)$) is represented in both red and blue channels (magenta), and finally when these images completely overlap we have the white color.

IV. Results and Experimental Evaluation

To validate the performance of our approach towards optimizing registration algorithms that are typically found in the field of fundus photography, we conduct a comprehensive experimental evaluation taking five state-of-the-art methods and a representative public benchmark. More precisely, we make use of the FIRE database [20] which contains 134 image pairs reflecting a considerable number of eye impairments and other aggravating factors such as the presence of noise, eye's involuntary movements, and visual anatomical changes. For each image pair, it's available a set of 10 corresponding points marked by a medical expert which is taken as "ground truth" to calculate the Mean Registration Error (MRE) [20] (given in pixels). We then assess the accuracies reached by the following registration methods with/without our boosting scheme: SURF [9] and SIFT [13] tuned with RANSAC [21] for outliers removal, GDB-ICP [10], ED-DB-ICP [12] and RIR-BS [22]. Finally, following [20], we also consider that an image pair is indeed registered whether the MRE score is at least less than 25.

A. Quantitative Evaluation

We start our experimental analysis by extracting basic statistics like *mean*, *median* and *standard deviation* for the MRE over all the evaluated methods in their usual and GC-optimized versions, i.e., when the methods are combined with our GC-driven scheme for optimal mapping selection. From the statistics listed in Table I, one can verify that GC leads to a significant improvement in the registration accuracy, attesting its good performance in all the measurements. For example, the error computed for the conventional algorithms GDB-ICP and ED-DB-ICP are reduced to approximately half when they are equipped with our boosting scheme.

Table I
STATISTICS OF THE REGISTRATION METHODS IN THEIR BOTH STANDARD AND GC-OPTIMIZED VERSIONS WHEN ASSESSED BY THE MRE MEASURE.

	SIFT-based		**SURF-based**		**GDB-ICP**		**ED-DB-ICP**		**RIRBS**	
	Standard	GC	Standard	GC	Standard	GC	Standard	GC	Standard	GC
Mean	6.5689	4.8962	6.1012	4.8187	10.301	5.9499	8.3293	4.3363	6.9646	4.4631
Median	4.5484	3.1705	3.8692	3.0966	8.7278	4.0437	6.5854	2.2714	5.1057	3.4790
Std	4.9817	4.6785	5.9422	4.6242	5.8711	4.8703	6.0571	5.1967	5.4473	3.0553

Table II
NUMBER OF REGISTERED IMAGES FOR DIFFERENT PARAMETERS OF THE MRE FOR BOTH STANDARD AND GC-DRIVEN REGISTRATION METHODS.

	SIFT-based		**SURF-based**		**GDB-ICP**		**ED-DB-ICP**		**RIRBS**	
	Standard	GC	Standard	GC	Standard	GC	Standard	GC	Standard	GC
Error <5	61	81	49	52	42	85	22	64	35	52
Error <10	91	99	64	67	67	97	60	94	57	67
Error <15	99	104	68	72	87	104	78	103	67	77
Error <20	110	113	70	75	96	113	96	114	71	79
Error <25	112	115	76	77	102	119	102	121	74	82

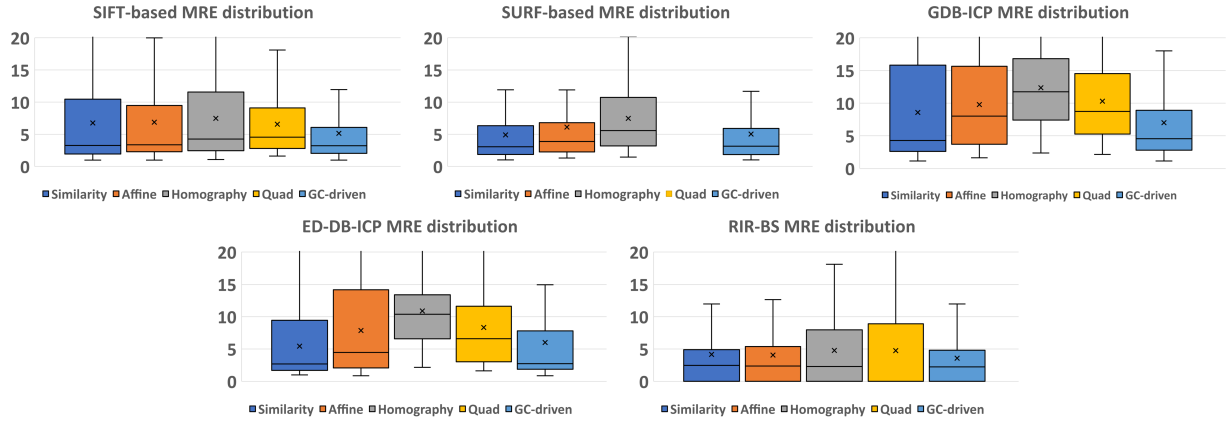

Figure 4. MRE for the registration methods when setting different geometric transformation models.

A deeper and more prescriptive evaluation concerning the registrations produced by the techniques can be visualized in Table II. Again, our GC-driven scheme significantly increases the accuracy performance for all the methods, performing a larger number of registrations even in more drastic cases such as the ones posed by low MRE thresholds. Another interesting aspect to be observed is that in certain circumstances, where a conventional method registers much more images than others, it is possible to reverse this scenario just by enabling the GC scheme into the second group of techniques (e.g., see SIFT-based vs. ED-DB-ICP).

In Figure 4, we assess the accuracy of the registration methods separately, i.e., by setting different transformations. More specifically, the methods are evaluated according to the following set of geometric models: *similarity*, *affine*, *homography*, *quadratic*, and, finally, by means of our GC-based decision rule. By checking the boxplots in Figure 4, one can see that the registrations delivered by our scheme have the lowest MRE values, in overall. The SURF method didn't return the minimum number of collinear points demanded to properly establish a quadratic model. We also compute in Figure 5 the frequency in which each geometric transformation is chosen as optimal by our GC scheme. The best choice measured by the MRE is also provided as "ground truth". The choices made by our approach follow the ones achieved by the MRE, being very stable regarding the MRE distribution for all the mappings. Another observed behavior for both GC and MRE metrics is that there is no absolute transformation to any registration method: they assume different models as the image pairs vary.

Next, we discuss how the designed GC scheme behaves in terms of *consistency* and "*smoothness*". Figure 6 displays the histogram of the geometric mappings chosen by our approach. Note that, as the best choice, GC highly maximizes the MRE, followed by the second-best choice, and so on. In other words, the registration methods driven by the GC scheme reach a good level of consistency, thus ensuring that the order of the "best-to-worst" choices for the geometric transformations will be preserved as much as possible. Also, GC presents a smooth response in the sense that the MRE peaks quickly decrease as the ranks fall.

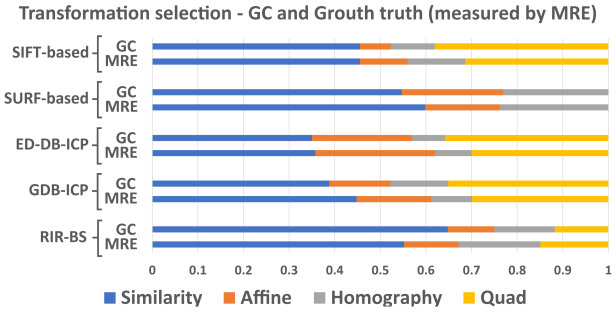

Figure 5. Number of times that a certain geometric transformation model is chosen as optimal by our CG scheme and the MRE.

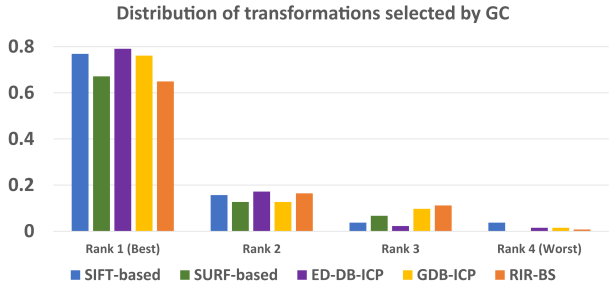

Figure 6. Number of transformations selected by the GC from best (Rank 1) to worst (Rank 4). Clearly, the histograms show that GC tends to determine the best transformations for each method.

B. Qualitative Analysis

We conclude this section showing in Figure 7 a qualitative set of results for a pair of retinal images. For each registration method, we consider two scenarios: the usual mappings, adopted by the current methods, versus the best competitor, as properly computed by our GC scheme. As shown from the visual and quantitative results measured by the MRE and CG, the proposed approach archives a satisfactory performance in terms of registration accuracy, varying from incremental to substantial improvements (e.g., see the SIFT and GDB-ICP examples).

V. Conclusion

In this paper, we introduce a new approach to improve the accuracy of fundus image registration methods. We revisit the decision of selecting the best geometric model for the registration task based on the image pair itself, and also from a novel overlapping metric designed to check the accuracy performance of the registered images. The proposed scheme is easy-to-code and it does not require any extra computational effort, as well as any "ground truth" annotation. From our experimental evaluations, we show that the results obtained by several well-established techniques for fundus image alignment can be substantively improved. Moreover, our approach presents very stable results when assessed by a ground truth-dependent metric, being also consistent in terms of registration accuracy.

As future work, we are currently studying registration methods based on machine learning approaches to properly deal with different kinds of pathologies, so we can create better tools for diagnostic assistance.

Acknowledgment

This research has been supported by FAPESP (grant #2013/07375-0), CNPq (grant #301642/2017-6) and CAPES (grant PROEX-7486558/D).

References

[1] M. A. Viergever, J. B. A. Maintz, S. Klein, K. Murphy, M. Staring, and J. P. Pluim, "A survey of medical image registration - under review," *Medical Image Analysis*, vol. 33, pp. 140–144, 2016.

[2] E. P. Ong, J. A. Lee, J. Cheng, B. H. Lee, G. Xu, A. Laude, S. Teoh, T. H. Lim, D. W. K. Wong, and J. Liu, "An augmented reality assistance platform for eye laser surgery," in *Annual International Conference of the IEEE Engineering in Medicine and Biology Society*, 2015, pp. 4326–4329.

[3] S. Philip, L. Cowie, and J. Olson, "The impact of the health technology board for scotlands grading model on referrals to ophthalmology services," *The British Journal of Ophthalmology*, vol. 89, no. 1, pp. 891–896, 2005.

[4] M. D. Abramoff, M. Niemeijer, M. S. Suttorp-Schulten, M. A. Viergever, S. R. Russell, and B. van Ginneken, "Evaluation of a system for automatic detection of diabetic retinopathy from color fundus photographs in a large population of patients with diabetes," *Diabetes Care*, vol. 33, no. 8, pp. 64–84, 2008.

[5] J. Pieczynski and A. Grzybowski, "Review of diabetic retinopathy screening methods and programmes adopted in different parts of the world," *European Ophthalmic Review*, vol. 9, no. 1, pp. 49–55, 2015.

[6] A. Sotiras, C. Davatzikos, and N. Paragios, "Deformable medical image registration: A survey," *IEEE transactions on medical imaging*, vol. 32, no. 7, pp. 1153–1190, 2013.

[7] J. A. Schnabel, M. P. Heinrich, B. W. Papież, and J. M. Brady, "Advances and challenges in deformable image registration: From image fusion to complex motion modelling," *Medical image analysis*, vol. 33, pp. 145–148, 2016.

[8] B. Zitov and J. Flusser, "Image registration methods: A survey," *Image and Vision Computing*, vol. 21, no. 11, pp. 977–1000, 2003.

[9] P. C. Cattin, H. Bay, L. V. Gool, and G. Szekely, "Retina mosaicing using local features," in *International Conference on Medical Image Computing and Computer-Assisted Intervention*, 2006, pp. 185–192.

[10] G. Yang, C. V. Stewart, M. Sofka, and C.-L. Tsai, "Registration of challenging image pairs: Initialization, estimation, and decision," *IEEE Trans. on PAMI*, vol. 29, no. 11, pp. 1973–1989, 2007.

[11] D. Rueckert and P. Aljabar, "Nonrigid registration of medical images: Theory, methods, and applications," *IEEE Signal Processing Magazine*, vol. 27, no. 4, pp. 113–119, 2010.

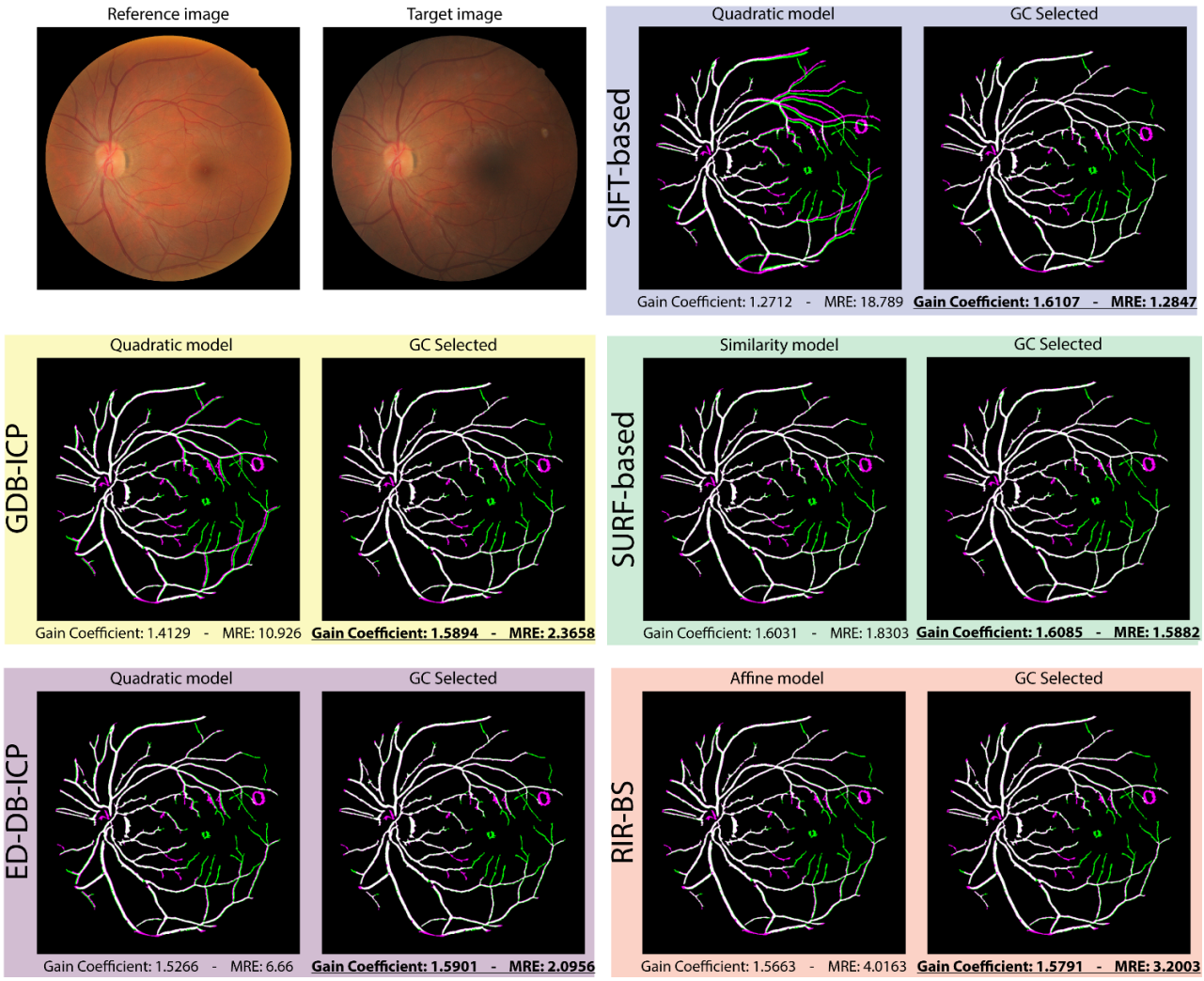

Figure 7. Qualitative comparison for a given image pair when assessed by all the five evaluated methods.

[12] C.-L. Tsai, C.-Y. Li, G. Yang, and K.-S. Lin, "The edge-driven dual-bootstrap iterative closest point algorithm for registration of multimodal fluorescein angiogram sequence," *IEEE Transactions on Medical Imaging*, vol. 29, no. 3, pp. 636–649, 2010.

[13] D. C. B. M and C. J. Moses, "Retinal image registration feature descriptors - a survey," in *IEEE International Conference on Electronics and Communication Systems*, 2014, pp. 1–5.

[14] S. Lee, J. M. Reinhardt, P. C. Cattin, and M. D. Abramoffade, "Objective and expert-independent validation of retinal image registration algorithms by a projective imaging distortion model," *Medical Image Analysis*, vol. 14, pp. 539–549, 2010.

[15] R. Varadhan, G. Karangelis, K. Krishnan, and S. Hui, "A framework for deformable image registration validation in radiotherapy clinical applications," *Journal of Applied Clinical Medical Physics*, vol. 14, no. 1, pp. 192–213, 2013.

[16] F. E.-Z. A. El-Gamal, M. Elmogy, and A. Atwan, "Current trends in medical image registration and fusion," *Egyptian Informatics Journal*, vol. 17, no. 1, pp. 99–124, 2016.

[17] R. Szeliski, *Computer Vision: Algorithms and Applications*, 1st ed. Springer-Verlag New York, Inc., 2010.

[18] S. M. Eldeeb and A. S. Fahmy, "Error analysis of fundus image registration using quadratic model transformation," in *Int. Biomedical Engineering Conference*, 2014, pp. 137–140.

[19] P. Bankhead, C. N. Scholfield, J. G. McGeown, and T. M. Curtis, "Fast retinal vessel detection and measurement using wavelets and edge location refinement," *PloS One*, vol. 7, no. 3, p. e32435, 2012.

[20] C. Hernandez-Matas, X. Zabulis, A. Triantafyllou, P. Anyfanti, S. Douma, and A. A. Argyros, "Fire: Fundus image registration dataset," *Journal for Modeling in Opthalmology*, vol. 1, no. 4, pp. 16–28, 2017.

[21] K. G. Derpanis, "Overview of the ransac algorithm," Computer Science, York University, Tech. Rep., 2010.

[22] L. Chen, Y. Xiang, Y. Chen, and X. Zhang, "Retinal image registration using bifurcation structures," in *IEEE International Conference on Image Processing (ICIP)*, 2011, pp. 2169–2172.